arXiv:1604.03718v2 [cond-mat.str-el] 18 Apr 2016

Stabilization of the tetragonal structure in $(Ba_{1-x}Sr_x)CuSi_2O_6$

Pascal Puphal,[1,*] Denis Sheptyakov,[2] Natalija van Well,[1,2] Lars Postulka,[1] Ivo Heinmaa,[3] Franz Ritter,[1] Wolf Assmus,[1] Bernd Wolf,[1] Michael Lang,[1] Harald O. Jeschke,[4] Roser Valentí,[4] Raivo Stern,[3] Christian Rüegg,[2,5] and Cornelius Krellner[1]

[1] *Physikalisches Institut, Goethe-Universität Frankfurt, 60438 Frankfurt am Main, Germany*
[2] *Laboratory for Neutron Scattering and Imaging, Paul Scherrer Institute, 5232 Villigen, Switzerland*
[3] *National Institute of Chemical Physics and Biophysics, 12618 Tallinn, Estonia*
[4] *Institut für Theoretische Physik, Goethe-Universität Frankfurt, 60438 Frankfurt am Main, Germany*
[5] *Department of Quantum Matter Physics, University of Geneva, 1205 Geneva, Switzerland*

We present a structural analysis of the substituted system $(Ba_{1-x}Sr_x)CuSi_2O_6$, which reveals a stable tetragonal crystal structure down to 1.5 K. We explore the structural details with low-temperature neutron and synchrotron powder diffraction, room-temperature and cryogenic high-resolution NMR, as well as magnetic- and specific-heat measurements and verify that a structural phase transition into the orthorhombic structure which occurs in the parent compound $BaCuSi_2O_6$, is absent for the $x = 0.1$ sample. Furthermore, synchrotron powder-diffraction patterns show a reduction of the unit cell for $x = 0.1$ and magnetic measurements prove that the Cu-dimers are preserved, yet with a slightly reduced intradimer coupling J_{intra}. Pulse-field magnetization measurements reveal the emergence of a field-induced ordered state, tantamount to Bose-Einstein-condensation (BEC) of triplons, within the tetragonal crystal structure of $I\,4_1/acd$. This material offers the opportunity to study the critical properties of triplon condensation in a simple crystal structure.

I. INTRODUCTION

Magnetic insulators with Cu^{2+} dimers are suitable materials to study quantum many-body effects under variable conditions. The occurrence of magnetic field-induced ordered states, which can be described as Bose-Einstein condensation (BEC) of triplons in this type of compounds provide a platform to study this ordered state in great detail, e.g., by investigating scaling laws of thermodynamic quantities [1]. The main idea behind this is that dimers of two Cu^{2+}-ions, which each carry a spin 1/2, can be mapped onto bosons to realize a BEC [2]. A prominent material where the appearance of a field-induced BEC of triplons was reported, is $BaCuSi_2O_6$ [3], owing its particular structure to layers of closed rings of SiO_4 tetrahedra bridged by vertically arranged Cu^{2+} dimers which form a square lattice (see Fig. 1). It was proposed that frustrated inter-dimer couplings between the dimer layers lead to a dimensional crossover at the quantum phase transition from a paramagnetic to a field-induced magnetically ordered state [4]. However, it is known since 2006, that $BaCuSi_2O_6$ undergoes a first-order structural phase transition at $T \sim 100K$ from a high-temperature tetragonal to a low-temperature orthorhombic symmetry, followed by a weak incommensurability of the crystal structure [6–8] which thus leads to two different kinds of dimers in adjacent layers. The impact of these two types of dimers on the peculiar properties of the reported BEC of triplons and the role of the frustration in this material are still under debate [7, 9, 10].

Mazurenko *et al.* [11] showed by performing density functional theory (DFT) calculations based on low-temperature structural data of the orthorhombic crystal structure, that the frustration between dimer layers is released due to the presence of a significant antiferromagnetic interaction between the upper site of one dimer and the bottom site of the neighbor dimer. Such a finding, backed by elastic neutron scattering data, questioned existing theories based on the presence of interlayer frustration. Recently, low-temperature high-resolution NMR (nuclear magnetic resonance) measurements [12] detected broadened ^{29}Si lines with complex line shape in the orthorhombic phase suggesting a more complex structure than originally thought, which complicates the understanding of the observed field-induced BEC of triplons at low temperatures.

In view of the existing controversy, we follow in this work a different strategy to avoid the influence of the structural phase transition. We present results of a successful partial substitution of Ba by Sr which reveals to a stable tetragonal phase of $BaCuSi_2O_6$ down to the lowest temperature of our experiment of 1.5 K. With only one type of dimers in the structure and the absence of structural modulations down to lowest temperatures, such systems allow for the investigation of the critical properties of field-induced ordered states without having to deal with complications from the crystal structure. We further present a detailed characterization of $Ba_{1-x}Sr_xCuSi_2O_6$ based on synchrotron and neutron diffraction measurements, NMR, thermodynamic measurements and DFT calculations and show that magnetization and susceptibility measurements for $Ba_{1-x}Sr_xCuSi_2O_6$ at $x = 0.1$ display a field-induced or-

dered state around 22 T.

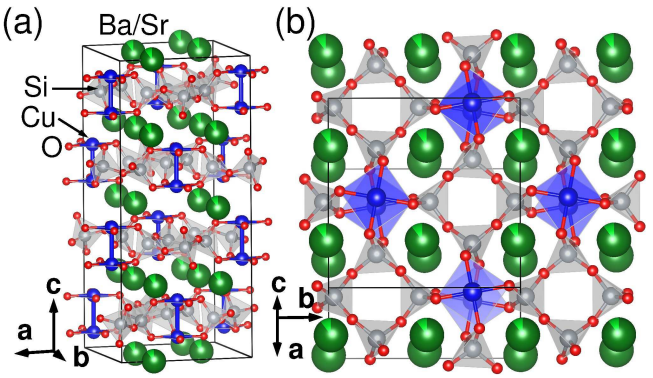

FIG. 1. $(Ba_{1-x}Sr_x)CuSi_2O_6$ structure for $x = 0.1$. (a) General view showing the arrangement of the Cu-dimers (blue) and the SiO_4 tetrahedrons (grey) (b) View close to the c-axis depicting the square lattice arrangement of the dimer layers, with highlighted CuO_4 plaquets (blue).

II. EXPERIMENTAL DETAILS

Polycrystalline $(Ba_{1-x}Sr_x)CuSi_2O_6$ powder samples were prepared by sintering $BaCO_3$, $SrCO_3$, CuO and SiO_2 where the initial weight percentage of $BaCO_3$ was substituted by 5, 10, 20 and 30% $SrCO_3$. The powder was ground and sintered in an aluminum oxide crucible in air at 1029°C (for 5%), 1028°C (for 10%), 1025°C and 1020°C for 2 months with several steps of grinding in between. Even after these long sintering times there is still a small amount ($< 5\%$) of impurities, which are the competing pre-phase $BaCu_2Si_2O_7$ and end-phase $BaCuSi_4O_{10}$, in the silicate formation [13]. We could not manage to synthesize compounds with Sr contents higher than 30%, but it also has to be noted that the pure $SrCuSi_2O_6$ phase has not been reported so far. Also a polycrystalline $BaCu(Si_{1-y}Ge_y)_2O_6$ powder sample with 10% of SiO_2 substituted by GeO_2 was obtained by sintering at 1027°C.

Single crystals were grown with pre-sintered $(Ba_{1-x}Sr_x)CuSi_2O_6$ powder spread in a boat-shaped platinum crucible. This crucible was placed in a tube furnace with an oxygen atmosphere of 1 bar where a viscous melt is reached at a temperature of 1150°C, followed by crystallization using a cooling rate of 12 K/h. Here the oxygen is used to suppress the decay of copper oxide $2CuO \rightarrow Cu_2O + \frac{1}{2}O_2$ as described previously [3]. The details of the crystal growth and the influence of oxygen atmosphere on the crystal structure will be reported elsewhere [5].

The pure $BaCuSi_2O_6$ crystals were grown in a platinum crucible with KBO_2 flux and a molar ratio of 1 : 2 (flux : powder) at 950 °C, where similar to [14], the crystallization starts as a consequence of an oversaturation caused by evaporation and some crawling due to a wetting of the crucible.

The powder diffraction experiments were carried out with two different diffraction techniques: the high-resolution powder neutron diffractometer HRPT [15] at the spallation neutron source SINQ and the Powder Diffraction station of the Materials Sciences Beamline (MS-PD) [16] at the Swiss Light Source, both at the Paul Scherrer Institute in Villigen. For the HRPT experiments, an amount of ~ 1 g of $Ba_{0.9}Sr_{0.1}CuSi_2O_6$ was enclosed into a vanadium can with an inner diameter of 6 mm and the measurement was carried out at room temperature, as well as at 1.5 K in a ^{4}He bath cryostat.

The synchrotron X-ray diffraction data were collected with the SLS-MS Powder Diffractometer on a powder sample enclosed in a capillary with a diameter of 0.3 mm, which was placed in a Janis flow-type cryostat (4 - 300 K). The Microstrip Mythen-II detector was used, which allowed for high counting rates while maintaining the high resolution which was essentially sample-conditioned. The typical counts of $\sim 2 \cdot 10^5$ in the strongest peaks were achieved within ~ 1 minute.

The high-resolution powder NMR-spectra were recorded with a Bruker AVANCE-II spectrometer attached to a 8.45 T magnet using home built MAS-NMR probes for 1.8 mm rotors at the National Institute of Chemical Physics and Biophysics in Tallinn. At room temperature spectra were recorded at 35 kHz sample spinning speed and at low temperatures they were recorded at about 30 kHz. At fast magic angle spinning (MAS) the broad NMR line of a powder sample transforms into the single peak at the isotropic value of the magnetic shift interaction [17]. If the spinning speed is less than the magnetic shift anisotropy in frequency units, then the main peak is accompanied by a number of spinning sidebands at multiples of the spinning speed value from the main peak. Although, the pattern of many spinning sidebands seems complicated, it tells us unambiguously how many inequivalent nuclear sites exist in the structure. The main purpose for using this technique here is to show, that there is only one silicon site in doped $BaCuSi_2O_6$ at room temperature and at low temperature as well, whereas the ^{29}Si MAS NMR spectrum of the parent compound shows the appearance of additional ^{29}Si resonance lines below $T < 100$ K [12].

Specific heat data were taken by using the standard option of a Physical Property Measurement System (PPMS) of Quantum Design with a high heating pulse technique discussed in chapter V.

The magnetic properties of several single crystals and a powder sample were determined in the temperature range $2\text{ K} \leq T \leq 300\text{ K}$ and in magnetic fields $B \leq 5$ T using a Quantum Design SQUID magnetometer. All data have been corrected for the temperature-independent diamagnetic core contribution of the constituents according to [20] and the magnetic contribution of the sample holder.

High-resolution magnetization measurements were performed in a capacitor-driven pulse-field setup with which experiments can be performed up to 58 T with a pulse duration of 21 ms. The setup was equipped with a ^{4}He-bath cryostat. The sample was placed in a 1266 stycast can with a diameter of 3 mm.

III. STRUCTURAL CHARACTERIZATION AT ROOM TEMPERATURE

We performed a refinement of the crystal structure parameters at room temperature by a combined analysis of neutron and synchrotron X-ray powder diffraction data. The neutron diffraction HRPT results on 1 g of $Ba_{0.9}Sr_{0.1}CuSi_2O_6$ powder are shown for the room temperature measurement in Fig. 2 (black curve). The underlying refinement of the tetragonal $I\,4_1/acd$ structure (red curve) fits well the measured data. Furthermore, we find a good agreement between the neutron data and the synchrotron data as shown in Table I ($x = 0.1$).

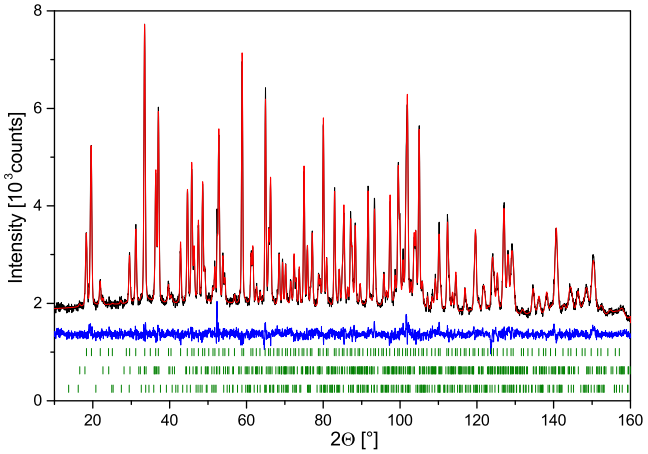

FIG. 2. Rietveld refinement of the crystal structure parameters of $(Ba_{1-x}Sr_x)CuSi_2O_6$ compound with a $x = 0.1$, based on neutron powder diffraction data at 300 K. The observed intensity (black), calculated profile (red), and difference curve (blue) are shown. The rows of ticks at the bottom correspond to the calculated diffraction peak positions of the phases (from top to bottom): $BaCuSi_2O_6$, $BaCu_2Si_2O_7$ (2.7% wt.) and $BaCuSi_4O_{10}$ (1.5% wt.).

In addition to the powder data, a crushed single crystal of $Ba_{0.9}Sr_{0.1}CuSi_2O_6$ was measured with synchrotron X-ray diffraction at room temperature and the measured data together with the refinement is shown in Fig. 3. We observe that the tetragonal structure is preserved at doping levels up to 30% at room temperature. The unit cell dimensions decrease with increasing strontium amount. This can be seen in a shift of the diffraction peaks to higher angles (see the inset in Fig. 3) and in the evolution of the unit cell parameters in Table I. This continuous evolution evidences that the Sr is built in, replacing the larger Ba atoms. In addition, the synchrotron data in the inset of Fig. 3 indirectly indicate a homogeneous distribution of strontium in the material, since the FWHM (full-width at half minimum) values show no significant increase with increasing strontium content. For example, the FWHM's of the (624) peak are 0.046°, 0.050°, 0.049° and 0.051° for compounds with x = 0.05, 0.1, 0.2 and 0.3 respectively. Comparing neutron data from a $BaCuSi_2O_6$ powder to the $x = 0.1$ powder we see that introducing Sr into the structure causes a slight peak broadening, which is qualitatively indicative to the presence of microstrains in the substituted materials. A further effect is that a decreased thermal expansion is observed, which influences the Cu-Cu distances and the different exchange couplings J at low temperatures in Table II.

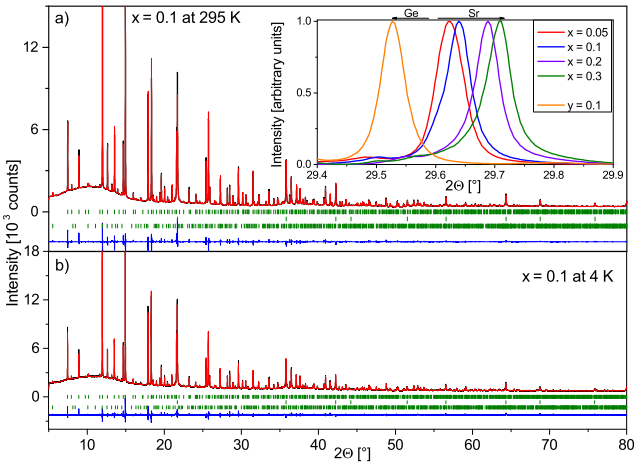

FIG. 3. Rietveld refinement of the crystal structure parameters of $(Ba_{1-x}Sr_x)CuSi_2O_6$ crushed single crystal with a $x = 0.1$, based on synchrotron X-ray powder diffraction data at a) 295 K and b) 4 K. The rows of ticks in the middle correspond to the calculated diffraction peak positions of the phases (from top to bottom): $BaCuSi_2O_6$, diamond powder (added to reduce the absorption) and $BaCuSi_4O_{10}$ (3.4 % wt.). The inset shows synchrotron X-ray powder diffraction data of the (624) peak measured at 295 K of polycrystalline samples with various substitution levels.

The results of all refinements and of the energy dispersive X-ray spectroscopy (EDX) measurements are presented in Table 1 and it is apparent, that the actual Sr content slightly varies from sample to sample. As a general trend, the amount of strontium, x, in the powder is lower than the nominal one and this value further decreases in the single crystals. The occupation refinement value x is compared to the data obtained from the EDX analysis in a Zeiss DSM 940A scanning electron microscope (SEM) on both powder and single crystals. The Sr content from the EDX measurement on the powder samples seems to be slightly overestimated compared to the value from the refinement. The reason for this is possibly related to Sr-enriched foreign phases, which increase

TABLE I. Summary of the refinement and EDX results of several samples of the series $(Ba_{1-x}Sr_x)CuSi_2O_6$ and a sample of $BaCu(Si_{1-y}Ge_y)_2O_6$. The abbreviations are as following: neutron diffraction (N), synchrotron diffraction (S), polycrystalline powder or crushed crystal (P), and single crystal sample (SC).

Nominal value	$x = 0.05$	$x = 0.1$					$x = 0.2$	$x = 0.3$	$y = 0.1$
Powder/ Single crystal	P	SC		P			P	P	P
x_{EDX} value	0.08(1)	0.08(2)		0.13(1)			0.19(2)	0.33(3)	0.08(2)
Neutron/ Synchrotron	S	S [18]		N [18]		S	S	S	S
$x_{refined}$ value	0.03	0.05		0.07		0.09	0.16	0.26	0.08
Temperature	295 K	295 K	4 K	300 K	1.5 K	295 K	295 K	295 K	295 K
a [Å]	9.97331(2)	9.97223(2)	9.95830(5)	9.9627(3)	9.9508(2)	9.95888(2)	9.94442(1)	9.93810(3)	9.9935(1)
c [Å]	22.30826(6)	22.31379(4)	22.3246(1)	22.2774(7)	22.2815(5)	22.27168(6)	22.23223(5)	22.2129(1)	22.4325(2)
V [Å^3]	2218.93	2219.08	2213.88	2210.58	2205.31	2208.89	2198.58	2193.88	2240.33

the amount of Sr in the EDX result, while in the refined results they are refined seperately. Also SrO impurities cannot be detected in diffraction experiments, since it decays and becomes amorphous. For clarity, we will use in the following the nominal values to describe the samples.

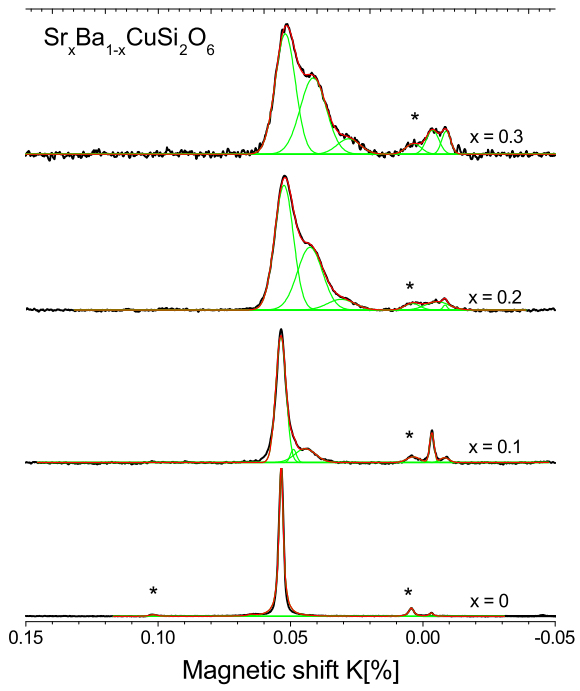

FIG. 4. ^{29}Si MAS-NMR spectra at $T = 300$ K with a resonance frequency of 71.5 MHz of ^{29}Si on $BaCuSi_2O_6$ (bottom spectrum) and Sr substituted $BaCuSi_2O_6$ as noted in the figure. The asterisks denote spinning side bands. Decomposition of the spectra can be seen by analyzing the green fitting curves. Homogeneous substitution of Ba by Sr is clearly reflected in the ^{29}Si MAS-NMR spectra.

To have a further insight into the distribution of Sr in the samples, room-temperature, high-resolution ^{29}Si-NMR measurements were done on the Sr-powder substitution series. The results of the chemical shift K are depicted in Fig. 4 and a broadening of the main peak around $K \sim 0.05\%$ is apparent. This line broadening can be explained, assuming a random distribution of Sr on the Ba sites. In $BaCuSi_2O_6$, each silicon atom, which is the probed NMR nuclei, has two Ba nearest neighbors. For the $x = 0.1$ compound the probability to have a silicon atom with two Ba neighbors is 0.81, with one Ba and one Sr 0.18, and with two Sr neighbors only 0.01, if Sr is homogeneously distributed over the Ba sites. Therefore, one would expect a peak splitting of the main ^{29}Si-NMR line into a triplet with an intensity ratio of (0.81 : 0.18 : 0.01). Looking at the spectra in Fig. 4, such a peak splitting is indeed observed. At 10% Sr concentration the spectrum shows the main line at 0.0536 % and a shoulder at 0.0444 %. The intensity ratio of these lines is (0.83 : 0.17), which is in nice agreement, with the expected splitting, although the peak with two Sr sites is below the detection limit.

The main lines in the spectrum of 20% Sr are positioned at 0.0526 %, 0.0427 % and 0.0310 % with an intensity ratio of (0.55 : 0.38 : 0.07), in rough correspondence with the expected site distribution, which would lead to a side distribution of (0.64 : 0.32 : 0.04). The main lines in the spectrum of 30% Sr substituted compound are at 0.0520 %, 0.0414 % and 0.0280 %. The intensity distribution of the lines (0.51 : 0.42 : 0.07) is again in good agreement with a random distribution of Sr sites (0.49 : 0.42 : 0.09).

IV. INVESTIGATION OF THE ABSENCE OF A STRUCTURAL PHASE TRANSITION

We discuss now the low-temperature diffraction data obtained both in measurements on powder as well as single crystal samples with the nominal Sr concentration $x = 0.1$. The absence of a structural phase transition down to the lowest measured temperatures could be ver-

ified in neutron and synchrotron diffraction. In Fig. 3 b) the Rietveld refinement of the same crushed single crystal as in Fig. 3 a) is presented for measurements at 4 K. This data set can be refined, using the same tetragonal crystal structure with space group $I\,4_1/acd$, which is observed also at room temperature. The corresponding results of the refinement are shown in Table I.

Further evidence for the absence of a structural phase transition is presented in Fig. 5, where the temperature-dependent synchrotron data across the expected transition temperature are shown. We choose the (604) and (620) reflexes in a temperature window from 10 to 110 K to make a comparison with Ref. [7] possible, where corresponding data were shown for $x = 0$. There, a well resolved peak splitting is observed as shown for comparison in the back of Fig. 5. In the whole temperature region for the $x = 0.1$ sample, no peak splittings or shifts beyond the expected thermal expansion could be observed. Similar results were obtained with neutron diffraction at 1.5 K, where on a polycrystalline sample, with slightly higher Sr concentration, also no structural phase transition could be detected. The same suppression of the phase transition was observed for a 10 % Ge doped powder sample ($y = 0.1$ in Table I) in synchrotron measurements in the range of 4 K $< T <$ 295 K.

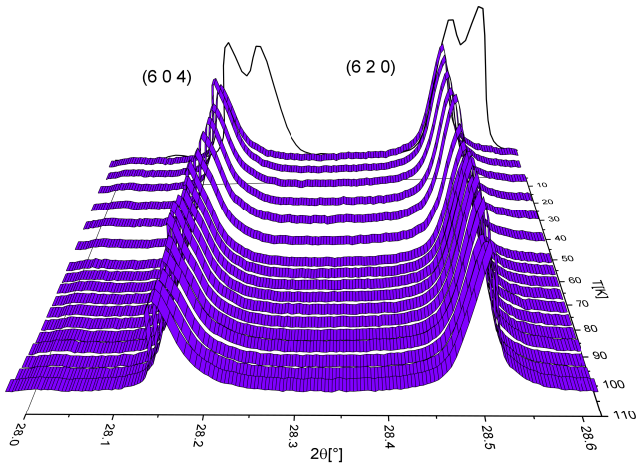

FIG. 5. Synchrotron X-ray powder diffraction data of an $x = 0.1$ crushed single crystal from 35 to 110 K. In the back a measurement of the $x = 0$ powder at 30 K is shown (black line), demonstrating how the peak splitting due to the transition would look like (data taken from of Ref. [7]). The suppression of the structural phase transition is apparent, since for $Ba_{0.9}Sr_{0.1}CuSi_2O_6$ the (604) and (620) reflexes do not split.

Next to the scattering experiments (sensitive to long-range structures), we also performed cryogenic high-resolution ^{29}Si NMR which show the absence of the transition in short-range correlations. The spectra show that, unlike the case of the parent compound $BaCuSi_2O_6$, where two different ^{29}Si resonance bands were found below the phase transition at T ∼96 K [12], there is clearly only one resonance line in the studied temperature range 37 K ≤ T ≤ 300 K (see figure 6). With lower temperatures there is a natural line broadening due to high magnetic suscebtibility of the powder particles which is not averaged by MAS, making the structure (shoulders) caused by Sr less and less detectable. The isotropic value of the ^{29}Si magnetic hyperfine shift in the $x = 0.1$ sample at room temperature for silicon with two Ba neighbors $K = 0.0536$ % is equal to the value in pure $BaCuSi_2O_6$ ($K = 0.0535$ %). In paramagnetic compounds the isotropic magnetic shift K is proportional to the magnetic suscebtibility χ_M as: $K = \frac{H_{hf}}{N_A g \mu_B}\chi_M$ where H_{hf} is the hyperfine field at the nucleus, N_A is the Avogadro's number, g and μ_B are the g-factor and the Bohr magneton, respectively. Equal magnetic hyperfine shifts result from equal hyperfine fields at silicon in $Ba_{0.9}Sr_{0.1}CuSi_2O_6$ and in the parent compound $BaCuSi_2O_6$.

A complementary measurement technique to detect first-order structural phase transitions is the heat capacity measured around the suspected phase transition. The advantages of this method are that the measurement is fast, the single crystals are kept intact and can be small. We measured specific heat data from 10 to 130 K with heating pulses of up to 10 K of single crystals with and without strontium substitution. As a consequence of the first-order nature of the structural transition in pure $BaCuSi_2O_6$, latent heat is expected, which easily can be detected as a small plateau during a continuous heating cycle (inset of Fig. 7) as described in Ref. [19]. This results in a diverging specific heat at the transition temperature as evident from the large peak in the main part of Fig. 7 (black curve). As this is a first-order transition, we observe a small satellite peak at higher temperatures, due to hysteresis effects upon heating and cooling. This anomaly is found to be absent for Sr-substituted samples, which is exemplarily shown for one $x = 0.1$ single crystal in Fig. 7 (red curve).

V. MAGNETIC CHARACTERIZATION

After having established that in Sr-substituted $BaCuSi_2O_6$ the structural transition into the orthorhombic structure is suppressed, the question arises, how these structural differences influence the magnetic properties at low temperatures and high magnetic fields. Here, we present magnetic susceptibility measurements on a $Ba_{0.9}Sr_{0.1}CuSi_2O_6$ single crystal down to 2 K together with high-field magnetization measurements up to 50 T at 1.5 K. For comparision, we also studied a single crystal of the undoped parent compound.

Using a SQUID magnetometer we determine the molar magnetic susceptibility of a $BaCuSi_2O_6$ single crystal of 8.79 mg. Futhermore we measured two $x = 0.1$ single crystals with masses of 4.07 mg (#1) and 5.29 mg (#2) and a $Ba_{0.9}Sr_{0.1}CuSi_2O_6$ powder sample of 110 mg

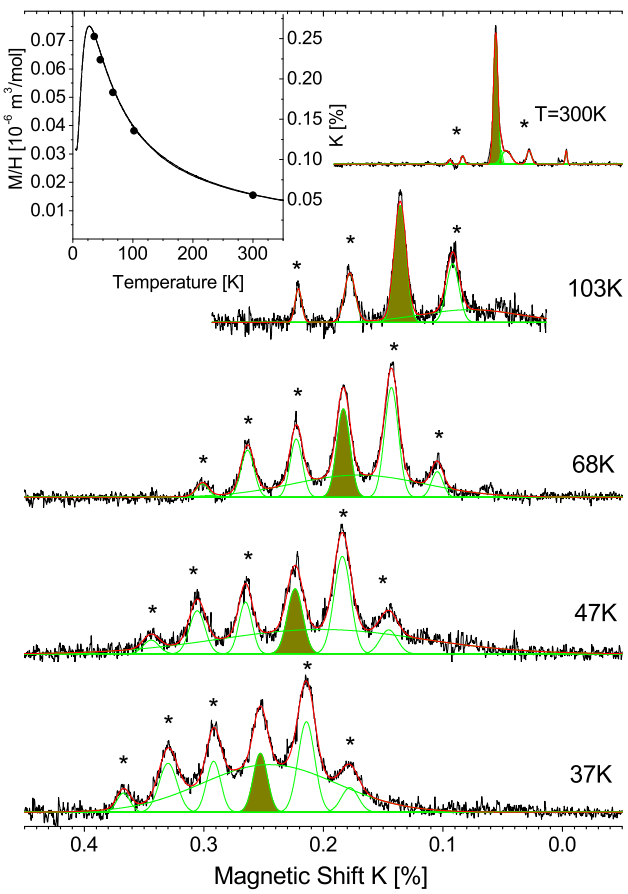

FIG. 6. The temperature dependence of ^{29}Si MAS-NMR spectrum of $Ba_{0.9}Sr_{0.1}CuSi_2O_6$. At magic-angle spinning the NMR spectra consist of the main line at isotropic magnetic shift and of a number of spinning sidebands at multiples of the sample-spinning frequency from the main line. For clarity the main lines in the spectra are colored and the spinning sidebands are marked with asterisks. The insert shows the proportionality of the isotropic magnetic shift to the molar susceptibility measured in a PPMS on the same sample at 8.45 T. Here the susceptibility values are given by the full line and circles correspond to the isotropic shift values.

in the temperature range $2\,\mathrm{K} \leq T \leq 300\,\mathrm{K}$ in a field of 1 T. A powder sample of this size ensures an optimal filling factor of the pick-up coil in the pulse-field experiments. In addition, we determine the magnetization of the powder up to 5 T at 2 K. The single crystals and the powder sample are of high quality as reflected by low paramagnetic (spin-1/2) impurity levels of 0.8 % for #1, 1.5 % for #2 and 5.5 % for the powder. For the undoped single crystal this spin-1/2 impurity level amounts to about 1.0 %. These impurities might arise from paramagnetic $BaCuSi_4O_{10}$ [23], observed in our x-ray and neutron diffraction data.

In a first attempt to extract the relevant magnetic coupling parameter J_{intra} (intradimer Cu-Cu exchange)

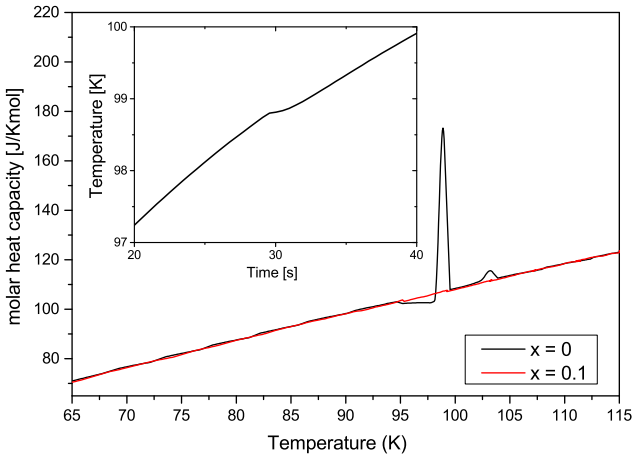

FIG. 7. Specific heat data of a $BaCuSi_2O_6$ single crystal grown in KBO_2 flux as well as a $Ba_{0.9}Sr_{0.1}CuSi_2O_6$ single crystal grown with oxygen partial pressure. The inset shows a single heat pulse in the vicinity of the structural phase transition of the $BaCuSi_2O_6$ single crystal.

(main panel of Fig. 8) and J_{inter} (average interdimer exchange) we performed combined fits of χ_m for $B_{\perp c}$ and $B_{\parallel c}$. For the g-factor, treated as the only independent parameter in fitting the two data sets, we obtained $g_{\perp c} = 2.07$ and $g_{\parallel c} = 2.32$. These are the typical values for Cu^{2+} ions in a square-planar environment [22]. For the antiferromagnetic intradimer coupling constant the fit yields $J_{\mathrm{intra}} = 46.7(5)$ K for #2 together with an antiferromagnetic coupling between dimers of $J_{\mathrm{inter}} = 10(2)$ K. For #1 (not shown) a fit of comparable quality results in slightly different values of $J_{\mathrm{intra}} = 47.7(5)\,\mathrm{K}$ and $J_{\mathrm{inter}} = 8(2)$ K. We believe that these differences in the magnetic coupling constants are due to deviations in the actual Sr concentrations from $x = 0.1$, as discussed above. These numbers can be compared with the results on the parent compound $BaCuSi_2O_6$. From fitting the data of the undoped single crystal in the same way as for crystals #1 and #2 (see the inset of Fig. 8 for $B_{\perp c}$) we obtain a sightly higher value for $J_{\mathrm{intra}} = 50.4(5)\,\mathrm{K}$ together with $J_{\mathrm{inter}} = 8(2)\,\mathrm{K}$ and a g-factor of 2.08. On the semi-logarithmic scale of the inset of Fig. 8 this small difference is directly visible in the shift of the maxima. Note, that these magnetic coupling constants are similar to the ones obtained in Ref. [3] where they were determined from the slope of the M(H) curves at 37 T for different temperatures using a Quantum Monte Carlo algorithm.

In Fig. 9 we show the results of the magnetization, M, as a function of magnetic field up to 50 T at a bath temperature of 1.5 K. In small fields we observe a mild increase of M which levels off at intermediate fields. We assign this to the Brillouin function of uncoupled Cu^{2+}(spin-1/2)-ions. By subtracting the corresponding contribution from the raw data we find zero magnetiza-

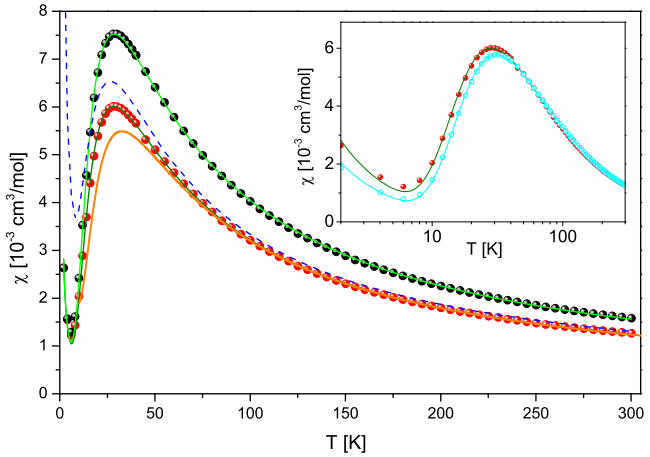

FIG. 8. Molar susceptibility of single crystal #2 for $B_{\perp c}$ (full red circles) and $B_{\parallel c}$ (full black circles) together with χ_m of the powder sample (blue broken line) measured as a function of temperature. Due to the random orientation of the micro crystals in the powder, its susceptibility lies between the data for $B_{\perp c}$ and $B_{\parallel c}$. The data of #2 for the different orientations are fitted with a random-phase approximation (RPA) according to [24] together with a Curie contribution resulting from isolated $S = \frac{1}{2}$ impurities (fits are the full green lines). The full orange line corresponds to the expected $\chi_m\,(T)$ using high-temperature series expansion (HTSE) [31] with the magnetic coupling constants taken from the DFT calculation, see chapter VI. Inset: $\chi\,(T)$of #2 (full red circles) together with the data of an undoped single crystal (open cyan circles) for $B_{\perp c}$. The solid lines are fits to the data using a RPA expression given in Ref. [24].

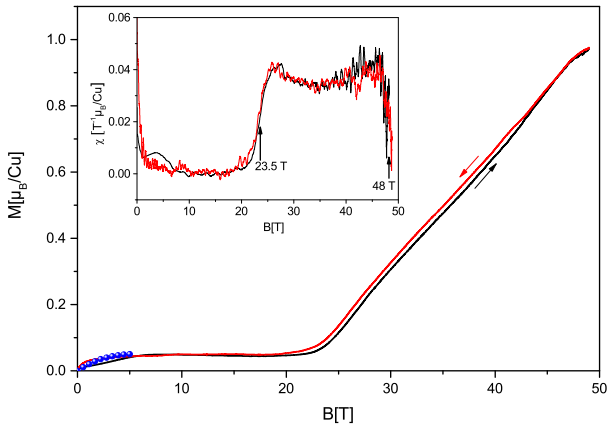

FIG. 9. Magnetization of the $Ba_{0.9}Sr_{0.1}CuSi_2O_6$ powder sample up to 50 T measured at a bath temperature of 1.5 K. The black solid line represents the data taken during increasing field with a rise time of 8 ms whereas the red solid line shows the magnetization with decreasing field with a decay time of 17 ms. The blue solid points are the SQUID data taken at 2 K. They follow a Brillouin-function corresponding to a concentration of 5.5 % uncoupled Cu^{2+}(spin-1/2)-ions. These data are used to calibrate the pulse-field experiments and they allow a rough estimate of the magnetocaloric effect which amounts to $\Delta T \simeq +1.5$ K for the field-up curve and $\simeq$ -0.5 K for the field-down curve with respect to the bath temperature.

tion up to a field of around 22 T. With further growing field, $M(B)$ increases almost linearly with B, until the saturation is reached at B_{c2} around 48 T. The small deviations between the field-up and field-down data are due to the magnetocaloric effect (MC), i.e., temperature changes due to changes of the magnetic field, in combination with the peculiar field-time characteristic of the pulse-field set up. The largest MC is expected for fields $\leq$ 5 T and around the critical fields B_{c1} and B_{c2}, with B_{c1} denoting the onset field of the field-induced order. In order to determine B_{c1}, we numerically differentiate the data and obtain the magnetic susceptibility, shown in the inset of Fig. 9. We define B_{c1} as the inflection point of the $\chi\,(B)$ curve in analogy to the criterion used in Ref. [3]. For the powder sample we obtain $B_{c1} = 23.5$ T at a temperature of about 2 K. This temperature is corrected for the MC. For a stack of single crystals (not shown here) we obtained a slightly smaller value of 22.3 T. Since B_{c1} scales with J_{intra}/g, a slight reduction observed in B_{c1} for the single crystals would be consistent with a 10% larger g-factor for fields perpendicular to the planes even though J_{intra} is slightly (maximally 5%) enhanced. As estimated in Ref. [11] a B_{c1} around 22 T corresponds to one of the dimer layers (layer A) in the orthorhombic low-temperature phase. This layer is structurally similar to the dimer layers in the tetragonal $I4_1/acd$ structure of $BaCuSi_2O_6$.

VI. ELECTRONIC STRUCTURE CALCULATIONS

In order to provide a more detailed analysis of the Cu-Cu interactions in $Ba_{0.9}Sr_{0.1}CuSi_2O_6$ beyond the $J_{\rm intra}$ and $J_{\rm inter}$ estimates from the previous section, we perform density functional theory calculations on the neutron and synchrotron diffraction refinements of 10% Sr doped $BaCuSi_2O_6$ samples (see Table I, $x = 0.1$) at room and low temperatures. We employ the all electron full potential local orbital (FPLO) code [26] using a generalized gradient approximation [27] exchange and correlation functional and correct for the strong correlations on the Cu^{2+} $3d$ orbitals with the GGA+U [28] functional. We lower the symmetry of $(Ba_{1-x}Sr_x)CuSi_2O_6$ from $I\,4_1/acd$ to $C\,2$ in order to make eight Cu sites inequivalent and calculate the total energies of 21 distinct spin configurations for each of the four structures. Note that the isoelectronic substitution of 10% Sr^{2+} for Ba^{2+} is reflected in the calculation only by the experimentally determined lattice constants and interatomic distances but not by actual replacement of Ba sites in a supercell approach. The 21 energies can be fitted [30] against five Heisenberg exchange couplings J_i with very

TABLE II. Calculated exchange couplings for the $(Ba_{1-x}Sr_x)CuSi_2O_6$ structures with nominal $x = 0.1$ given in Table 1. A GGA+U functional with $U = 8$ eV and $J_H = 1$ eV is used. The abbreviations are neutron diffraction (N) and synchrotron diffraction (S). In addition, couplings for pure tetragonal $BaCuSi_2O_6$ (structure from Ref. 33) are given in the last two lines.

	T (K)	J_1 (K)	J_2 (K)	J_3 (K)	J_4 (K)	J_5 (K)
N	1.5	51.6(1)	-0.27(1)	-0.41(1)	0.0(1)	7.9(1)
	300	58.6(1)	-0.27(2)	-0.35(1)	0.0(1)	8.3(1)
S	4	60.2(1)	-0.25(1)	-0.41(1)	0.0(1)	8.0(1)
	295	56.7(1)	-0.28(4)	-0.29(3)	0.0(1)	8.3(3)
$x = 0$	200	58.7(1)	-0.23(1)	-0.39(1)	0.0(1)	8.4(1)
$x = 0$ [11]	300	53	-0.3	-0.4	–	7.9

high accuracy, leading to very small error bar from the statistics. Note that the sub-Kelvin error bars result from the particularly well defined $S = \frac{1}{2}$ moments of Cu in $BaCuSi_2O_6$, leading to very precise mapping of the 21 DFT total energies to the Hamiltonian with five exchange couplings. The results for GGA+U interaction parameters $U = 8$ eV and $J_H = 1$ eV are given in Table II. The parameters $U = 8$ eV and $J_H = 1$ eV are chosen on the upper end of the interaction parameter range $U \in [6, 8]$ eV considered in previous studies for Cu^{2+} in square-planar oxygen environment [29, 32]. The five exchange paths are visualized in Fig. 10. $J_{\rm intra}$ as introduced in the previous section, corresponds to J_1 while $J_{\rm inter}$ corresponds to a non-trivial average of inter-dimer Cu-Cu interactions including J_2, J_3, J_4 and J_5. In Table II we also show the calculated exchange parameters for the $x = 0$ structure at 200 K (Ref. [33]) and include, for comparison, the results calculated in Ref. [11] for the room-temperature tetragonal $BaCuSi_2O_6$. We observe (i) a good agreement between our estimates and those of Ref. [11] for $x = 0$ in the tetragonal phase and (ii) a reasonably good agreement between our *ab initio*-calculated intradimer J_1 and $J_{\rm intra}$ obtained in the previous section. We use a high-temperature series expansion [31] in order to check if the calculated exchange couplings can explain the experimentally measured susceptibility. The values we obtain for the T = 1.5 K neutron structure produce the orange curve in Fig. 8, with a maximum at 31 K in good agreement to the experimental maximum at 32.5 K. (iii) Our calculation of the Hamiltonian parameters for the low temperature tetragonal structure of $Ba_{1-x}Sr_xCuSi_2O_6$ at nominal $x = 0.1$ show that the exchange interactions remain very similar to the couplings of the $T = 200$ K tetragonal structure of $BaCuSi_2O_6$. Clearly $Ba_{0.9}Sr_{0.1}CuSi_2O_6$, as well as the tetragonal $I4_1/acd$ $BaCuSi_2O_6$ phase display strong intradimer antiferromagnetic Cu-Cu couplings (J_1) and significant nearest-neighbor dimer top-bottom antiferromagnetic couplings (J_5) that release any type of possible frustration between dimer layers.

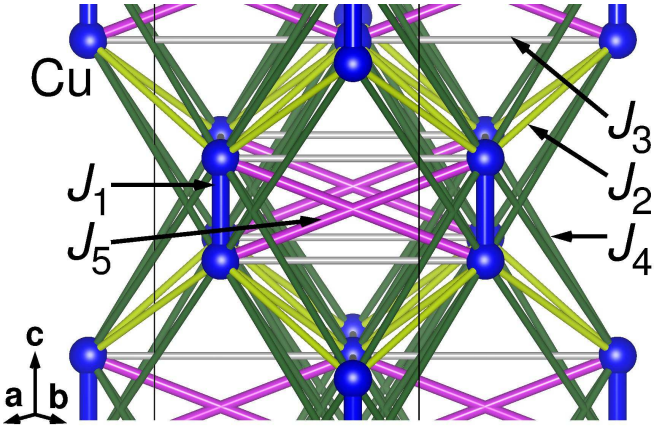

FIG. 10. Detail of the $BaCuSi_2O_6$ unit cell with the first five exchange paths between Cu^{2+} ions. Other ions are omitted for clarity.

VII. CONCLUSIONS

We have experimentally confirmed the absence of a first-order tetragonal-to-orthorhombic structural phase transition in $(Ba_{1-x}Sr_x)CuSi_2O_6$ by means of powder synchrotron X-ray and neutron diffraction, NMR, thermodynamic measurements and density functional theory calculations. We find that such a phase transition is suppressed with strontium substitution. Furthermore, the unit-cell volume decreases with increasing Sr content and the intradimer magnetic coupling becomes slightly reduced. Our DFT calculations for $x = 0.1$ for the tetragonal $I4_1/acd$ structures show the presence of strong antiferromagnetic Cu-Cu intradimer couplings and non-negligible antiferromagnetic nearest-neighbor dimer top-bottom antiferromagnetic couplings that avoid any kind of frustration between the dimer layers. The fact that for the germanium substituted sample the phase transition is also suppressed leaves us with a readily tunable system by varying the substitution concentrations. First high-field magnetic measurements on a powder sample with $x = 0.1$ at 2 K reveal clear indications for a field-induced ordered state, similar to the observations reported for the $x = 0$ parent compound. In contrast to the $x = 0$ material, however, where the analysis of the critical properties are plagued by uncertainties related to the presence of two sorts of dimers as a consequence of the structural transition, the $x = 0.1$ material is free of this complication. Therefore, detailed high-field measurements on this new material may help to clarify the influence of structural subtleties on the critical behavior of the field-induced order.

The authors gratefully acknowledge support by the Deutsche Forschungsgemeinschaft through grant SFB/TR 49 and project WE-5803/1-1. The work in Tallinn was supported by Estonian Research Council grants PUT210 and IUT23 – 7. This work is partly based on

experiments performed at the Swiss spallation neutron source SINQ, and the Swiss Light Source synchrotron radiation source at Paul Scherrer Institute, Villigen, Switzerland.

* puphal@physik.uni-frankfurt.de

[1] V. Zapf, M. Jaime, and C. D. Batista, *Bose-Einstein condensation in quantum magnets*, Rev. Mod. Phys. **86**, 563 (2014).

[2] T. Giamarchi, C. Rüegg, and O. Tchernyshyov, *Bose-Einstein condensation in magnetic insulators*, Nature Phys. **4**, 198 (2008).

[3] M. Jaime, V. F. Correa, N. Harrison, C. D. Batista, N. Kawashima, Y. Kazuma, G. A. Jorge, R. Stern, I. Heinmaa, S. A. Zvyagin, Y. Sasago, and K. Uchinokura, *Magnetic-Field-Induced Condensation of Triplons in Han Purple Pigment $BaCuSi_2O_6$*, Phys. Rev. Lett. **93**, 087203 (2004).

[4] S. E. Sebastian, N. Harrison, C. D. Batista, L. Balicas, M. Jaime, P. A. Sharma, N. Kawashima, and I. R. Fisher, *Dimensional reduction at a quantum critical point*, Nature **441**, 617 (2006).

[5] N. V. Well *et. al.* to be published

[6] E. C. Samulon, Z. Islam, S. E. Sebastian, P. B. Brooks, M. K. McCourt, Jr., J. Ilavsky, and I. R. Fisher, *Low-temperature structural phase transition and incommensurate lattice modulation in the spin-gap compound $BaCuSi_2O_6$*, Phys. Rev. B **73**, 100407 (2006).

[7] D. V. Sheptyakov, V. Yu. Pomjakushin, R. Stern, I. Heinmaa, H. Nakamura and T. Kimura, *Two types of adjacent dimer layers in the low-temperature phase of $BaCuSi_2O_6$*, Phys. Rev. B **86**, 014433 (2012).

[8] S. Krämer, R. Stern, M. Horvatić, C. Berthier, T. Kimura, and I. R. Fisher, *Nuclear magnetic resonance evidence for a strong modulation of the Bose-Einstein condensate in $BaCuSi_2O_6$*, Phys. Rev. B **76**, 100406 (2007).

[9] S. Krämer, R. Stern, M. Horvatić, C. Berthier, H. Nakamura and T. Kimura, *Spatially Resolved Magnetization in the Bose-Einstein Condensed State of $BaCuSi_2O_6$: Evidence for Imperfect Frustration*, Phys. Rev. B **87**, 180405 (2013).

[10] N. Laflorencie and F. Mila, *Theory of the field-induced BEC in the frustrated spin-$\frac{1}{2}$ dimer compound $BaCuSi_2O_6$*, Phys. Rev. Lett. **102**, 060602 (2009).

[11] V. V. Mazurenko, M. V. Valentyuk, R. Stern, and A. A. Tsirlin, *Nonfrustrated interlayer order and its relevance to the Bose-Einstein condensation of magnons in $BaCuSi_2O_6$*, Phys. Rev. Lett. **112**, 107202 (2014).

[12] R. Stern, I. Heinmaa, E. Joon, A. A. Tsirlin, H. Nakamura, T. Kimura, *Low-Temperature High-Resolution Solid-State (cryoMAS) NMR of Han Purple $BaCuSi_2O_6$*, Appl. Magn. Reson. **45**, 1253 (2014).

[13] H. Berke, *The invention of blue and purple pigments in ancient times*, Chem. Soc. Rev. **36**, 15 (2007).

[14] S. E. Sebastian, P. Tanedo, P. A. Goddard, S.-C. Lee, A. Wilson, S. Kim, S. Cox, R. D. McDonald, S. Hill, N. Harrison, C. D. Batista, and I. R. Fisher, *Role of anisotropy in the spin-dimer compound $BaCuSi_2O_6$*, Phys. Rev. B **74**, 180401R (2006).

[15] P. Fischer, G. Frey, M. Koch, M. Koönnecke, V. Pomjakushin, J. Schefer, R. Thut, N. Schlumpf, R. Buürge, U. Greuter, S. Bondt, E. Berruyer, *High-resolution powder diffractometer HRPT for thermal neutrons at SINQ*, Physica B **276**, 146 (2000).

[16] http://www.psi.ch/sls/ms/ms.

[17] E. R. Andrew, A. Bradbury, R. G. Eades, Nature 183, 1802 (1959).

[18] Selected structure files can be found in the Supplemental Information.

[19] J. C. Lashley, M. F. Hundley, A. Migliori, J. L. Sarrao, P. G. Pagliuso, T. W. Darling, M. Jaime, J. C. Cooley, W. L. Hults, L. Morales, D. J. Thoma, J. L. Smith, J. Boerio-Goates, B. F. Woodfield, G. R. Stewart, R. A. Fisher, N. E. Phillips, *Critical examination of heat capacity measurements made on a Quantum Design physical property measurement system*, Cryogenics **43**, 369-378 (2003).

[20] O. Kahn, *Molecular Magnetism*, VCH, Weinheim-New York (1993).

[21] S. Sasago, K. Uchinokura, A. Zheludev, and G. Shirane, *Temperature-dependent spin gap and singlet ground state in $BaCuSi_2O_6$*, Phys. Rev. B **55**, 8357 (1997).

[22] M. F. Ottaviani, F. Montalti, N.J. Turro, D.A. Tomalia, *Characterization of Starburst Dendrimers by the EPR Technique. Copper(II) Ions Binding Full-Generation Dendrimers*, J. Phys. Chem. B **101**, 158 (1997).

[23] S.H. Masunaga, A. Rebello, A.T. Schye, N. Prasai, J.J. Neumeier, J.L. Cohn, *Heat capacity, thermal expansion and heat transport in the Han Blue ($BaCuSi_4O_{10}$): Observation of structural phase transitions*, Journal of Physics and Chemistry of Solids **85**, 69–74 (2015)

[24] B. Lüthi, *Physical Acoustics in the Solid State*, Springer (2004).

[25] S. A. Zvyagin,, J. Wosnitza, J. Krzystek, R. Stern, M. Jaime, Y. Sasago, K. Uchinokura, *Spin-triplet excitons in the $S=\frac{1}{2}$ gapped antiferromagnet $BaCuSi_2O_6$: Electron paramagnetic resonance studies*, Phys. Rev. B **73**, 094446 (2006).

[26] K. Koepernik and H. Eschrig, *Full-potential nonorthogonal local-orbital minimum-basis band-structure scheme*, Phys. Rev. B **59**, 1743 (1999); http://www.FPLO.de.

[27] J. P. Perdew, K. Burke, and M. Ernzerhof, *Generalized Gradient Approximation Made Simple*, Phys. Rev. Lett. **77**, 3865 (1996).

[28] A. I. Liechtenstein, V. I. Anisimov, and J. Zaanen, *Density-functional theory and strong interactions: Orbital ordering in Mott-Hubbard insulators*, Phys. Rev. B **52**, R5467(R) (1995).

[29] H. O. Jeschke, F. Salvat-Pujol, and R. Valentí, *First-principles determination of Heisenberg Hamiltonian parameters for the spin-1/2 kagome antiferromagnet $ZnCu_3(OH)_6Cl_2$*, Phys. Rev. B **88**, 075106 (2013).

[30] U. Tutsch, B. Wolf, S. Wessel, L. Postulka, Y. Tsui, H. O. Jeschke, I. Opahle, T. Saha-Dasgupta, R. Valentí, A. Brühl, K. Remović-Langer, T. Kretz, H.-W. Lerner, M. Wagner, M. Lang, *Evidence of a field-induced Berezinskii-Kosterlitz-Thouless scenario in a two-dimensional spin-dimer system*, Nat. Commun. **5**, 5169 (2014).

[31] A. Lohmann, H.-J. Schmidt, J. Richter, *Tenth-order high-temperature expansion for the susceptibility and the specific heat of spin-s Heisenberg models with arbitrary exchange patterns: Application to pyrochlore and kagome magnets*, Phys. Rev. B **89**, 014415 (2014).

[32] H. O. Jeschke, F. Salvat-Pujol, E. Gati, N. H. Hoang, B. Wolf, M. Lang, J. A. Schlueter, and R. Valentí, *Barlowite as a canted antiferromagnet: theory and experiment*, Phys. Rev. B **92**, 094417 (2015).

[33] K. Sparta, *Structural Investigation of Quaternary Copper Oxides with Low Dimensional Magnetic Properties*, Ph.D. thesis, RWTH Aachen 2003.